Journal of Materials Chemistry A

Amorphous NiFe layered double hydroxide nanosheets decorated on 3D nickel phosphide nanoarrays: a hierarchical core-shell electrocatalyst for efficient oxygen evolution

Journal:	*Journal of Materials Chemistry A*
Manuscript ID	TA-ART-03-2018-002967.R2
Article Type:	Paper
Date Submitted by the Author:	24-Apr-2018

Complete List of Authors:	Yu, Luo; Central China Normal University, College of Physical Science and Technology; University of Houston, Department of Physics and TcSUH Zhou, Haiqing; University of Houston, Department of Physics Sun, Jingying; University of Houston, Physics Mishra, Ishwar; University of Houston, Department of Physics Luo, Dan; University of Houston, Department of Physics and TcSUH Yu, Fang; University of Houston, Department of Physics and TcSUH Yu, Ying; Central China Normal University, Institute of Nanoscience and Nanotechnology Chen, Shuo; University of Houston, Department of Physics and TcSUH Ren, Zhifeng ; University of Houston, Physics

Journal Name

ARTICLE

Amorphous NiFe layered double hydroxide nanosheets decorated on 3D nickel phosphide nanoarrays: a hierarchical core-shell electrocatalyst for efficient oxygen evolution

Received 00th January 20xx,
Accepted 00th January 20xx

DOI: 10.1039/x0xx00000x

www.rsc.org/

Luo Yu,[ab] Haiqing Zhou,[b] Jingying Sun,[b] Ishwar Kumar Mishra,[b] Dan Luo,[b] Fang Yu,[b] Ying Yu,*[a] Shuo Chen*[b] and Zhifeng Ren*[b]

The rational design of efficient and earth-abundant electrocatalysts for oxygen evolution reaction (OER) plays a paramount role in hydrogen production by water electrolysis. Here we report a 3D hierarchical core-shell nanostructured OER electrocatalyst, where amorphous NiFe layered double hydroxide (LDH) nanosheets are decorated on 3D conductive nickel phosphide nanoarrays. The integrated 3D core-shell electrode simultaneously offers excellent electrical conductivity for fast electron transfer, large surface area with numerous active edge sites, and hierarchical nanostructure for rapid release of gas bubbles, thus contributing to outstanding catalytic performance: low overpotentials (197, 243, and 283 mV for current densities of 10, 100, and 300 mA cm^{-2}, respectively), small Tafel slope (46.6 mV dec^{-1}), and superior stability, which is better than almost all the reported LDH-based OER catalysts. When combined this hybrid catalyst with the nickel phosphide for overall water splitting, the two-electrode cell achieves current densities of 10 mA cm^{-2} at 1.52 V and 100 mA cm^{-2} at 1.68 V in the alkaline media, which is even superior to the benchmark of IrO_2 and Pt. This work paves an effective approach to design 3D hierarchical hybrid electrocatalysts for energy conversion and storage.

Introduction

Renewable and clean energy is highly sought-after due to the grand challenge of energy crisis and environmental issues.[1-3] Electrochemical water splitting is a promising approach to store electric energy in clean energy of hydrogen. Unfortunately, its large-scale application is hampered by the sluggish kinetics of the oxygen evolution reaction (OER), which involves multistep proton and electron transfer processes with high overpotential and low efficiency.[4-6] To achieve high-performance OER, efficient electrocatalysts are required.[7, 8] Although Ir- and Ru-based materials show good OER performance, the high price and scarcity limit their practical utilization.[9-12] Therefore, enormous efforts have been devoted to developing competitive alternatives with earth abundance and low cost, which includes transition-metal oxides,[13] sufides,[14] selenides,[15] phosphides,[16] nitrides,[5] oxalates,[17] and (oxy)hydroxides,[7, 18] etc. However, the overpotential to deliver a current density of 10 mA cm^{-2} for these electrocatalysts is still more than 200 mV, not to mention that at 100 mA cm^{-2} or larger current densities. Thus, there is still urgent need for improvement of OER catalysts.

It is generally acknowledged that efficient OER electrocatalysts must possess abundant active sites for the adsorption/desorption process, excellent electrical conductivity for fast electron transfer, and robust nanostructure for long-term stability.[19, 20] Currently, layered double hydroxide (LDH)-based electrocatalysts have attracted much attention as a promising candidate for water splitting because of their unique layered structure, low cost, and ease of scale-up.[21-24] Nevertheless, their OER performance is inherently limited by the sparse catalytic edge sites and poor electrical conductivity.[25] In this sense, many strategies including exfoliation to obtain ultrathin nanosheets,[26] ion intercalation, and doping to tune the electronic properties[23, 27, 28] have been employed to improve the intrinsic OER activity of LDH-based catalysts. The treated LDH catalysts normally exhibit enhanced OER activity, but the performance is still unsatisfied. Moreover, the synthesis methods are typically time consuming, high-cost, and requiring polymer binder or conductive additives, which are not favorable for large-scale application.[25] Particularly, it has been confirmed that the active sites of two-dimensional (2D) layered materials are located at the edges rather than the basal planes,[29-31] so it is highly desired to grow LDH with numerous exposed edges, which can be achieved by growing the catalysts on a rough surface.[30, 32] In addition, 3D hierarchical architectures supported on conductive skeletons are of great interest due to the large surface area, efficient electron transfer, and rapid release of gas bubbles.[33, 34]

[a]*College of Physical Science and Technology, Central China Normal University, Wuhan 430079, China. Email: yuying01@mail.ccnu.edu.cn*
[b]*Department of Physics and TcSUH, University of Houston, Houston, TX 77204, United States. Email: schen34@uh.edu, zren@uh.edu*
†Electronic Supplementary Information (ESI) available: experimental details and results. See DOI: 10.1039/x0xx00000x

In view of these points, here we grow NiFe LDH nanosheets on highly conductive nickel phosphide nanoarrays to rationally design a 3D hierarchical core-shell nanostructured electrocatalyst,[35] which takes advantage of the superior conductivity and rough surface from the nickel phosphide foam, unique 3D hierarchical core-shell nanostructure with a large number of exposed edge sites, and strong structural integrity. As a result, the 3D hierarchical core-shell electrode exhibited excellent OER performance in alkaline media, where current densities of 10, 100, and 300 mA cm^{-2} at extremely low overpotentials of 197, 243, and 283 mV, respectively were achieved, together with a small Tafel slope of 46.6 mV dec^{-1} and good durability. This work provides an interesting route to rationally design efficient electrocatalysts from the 2D layered materials for electrochemical applications.

Results and discussion

Fig. 1a shows the fabrication process of the 3D hierarchical core-shell electrode, which begins with the growth of nickel phosphide nanoarrays from commercial Ni foam by direct phosphorization, following by electrodeposition of NiFe LDH nanosheets on the as-prepared nickel phosphide. From the X-ray diffraction (XRD) patterns

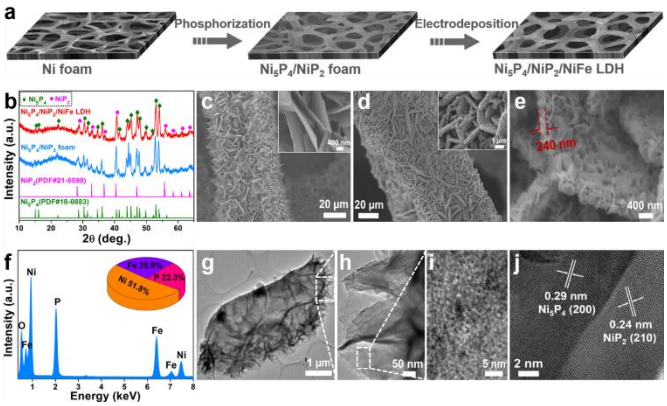

Fig. 1 (a) Schematic fabrication procedure of the 3D hierarchical core-shell $Ni_5P_4/NiP_2/NiFe$ LDH electrode. (b) XRD patterns of Ni_5P_4/NiP_2 foam and $Ni_5P_4/NiP_2/NiFe$ LDH. SEM images of (c) Ni_5P_4/NiP_2 nanoarrays, and (d,e) $Ni_5P_4/NiP_2/NiFe$ LDH at different magnifications. (f) EDX spectrum, (g,h) TEM images, and (i,j) HRTEM images of $Ni_5P_4/NiP_2/NiFe$ LDH.

in Fig. 1b, we can see that Ni foam was completely transformed into metallic nickel phosphide foam with a mixture of Ni_5P_4 (PDF#18-0883) and NiP_2 (PDF#21-0590) after the thermal phosphorization. After electrodeposition of NiFe LDH nanosheets, no new peaks emerged, which was because that the deposited NiFe LDH was amorphous. Fig. S1 (Supplementary Information) shows the scanning electron microscopy (SEM) images of commercial Ni foam, which possessed a macroporous skeleton with a flat surface. After phosphorization, the obtained Ni_5P_4/NiP_2 foam showed a nanoporous structure with a uniform vertical-aligned microsheet morphology (Fig. 1c), and the high magnification SEM image inserted in Fig. 1c further revealed that there were many voids between the microsheets. After the growth of NiFe LDH, the Ni_5P_4/NiP_2 microsheets were uniformly decorated by many well-organized nanosheets, yielding a desired highly porous and hierarchical core-shell nanostructure (Fig. 1d). From the high magnification SEM image in Fig. 1e, we observed that the NiFe LDH nanosheets were interconnected with each other to form a 3D ordered network with abundant exposed edges. Meanwhile, the large interspace between the neighboring arrays was clearly seen, which was favorable for electrolyte diffusion and gaseous product release.[29] The thickness of the whole hybrid microsheets was about 240 nm. It should be mentioned that the thickness of NiFe LDH shell and total morphology can be easily tuned by controlling the electrodeposition time, as illustrated in Fig. S2. Pure NiFe LDH was also synthesized on the Ni foam for comparison, and the SEM images in Fig. S3 showed a typically nanosheet array morphology. Fig. 1f shows the SEM energy dispersive X-ray (EDX) spectrum, confirming the existence of Ni, Fe, and P elements for the $Ni_5P_4/NiP_2/NiFe$ LDH hybrid, and the atomic ratio of Ni:Fe:P was about 1 : 0.5 : 0.43. The hierarchical core-shell nanostructure of the $Ni_5P_4/NiP_2/NiFe$ LDH hybrid microsheets were further investigated by transmission electron microscopy (TEM). As shown in Fig. 1g, we observed that the Ni_5P_4/NiP_2 microsheets were decorated by many leaf-like NiFe LDH nanosheets, and the hierarchical core-shell nanostructure can be easily distinguished. Moreover, the NiFe LDH shell vertically anchored on the surface of Ni_5P_4/NiP_2 microsheets composed of numerous ultrathin nanosheets with densely wrinkled feature, offering more active edge sites (Fig. 1h). High-resolution TEM (HRTEM) image in Fig. 1i (taken from the squared part of Fig. 1h) showed the amorphous nature of NiFe LDH shell, which was in agreement with the XRD result. HRTEM image in Fig. 1j further revealed distinctive lattice fringes with interplanar spacing of 0.24 and 0.29 nm, which were attributed to the (210) plane of NiP_2 and (200) plane of Ni_5P_4, respectively.

To ascertain the surface chemical states and elemental compositions of the as-prepared samples, X-ray photoelectron spectroscopy (XPS) measurements were conducted. As shown in Fig. 2a, the XPS survey spectra confirmed the presence of Ni, P, O, and C (for calibration) elements in both Ni_5P_4/NiP_2 foam and $Ni_5P_4/NiP_2/NiFe$ LDH, and Fe element was clearly shown in the XPS spectra of $Ni_5P_4/NiP_2/NiFe$ LDH. It should be noted that the peak

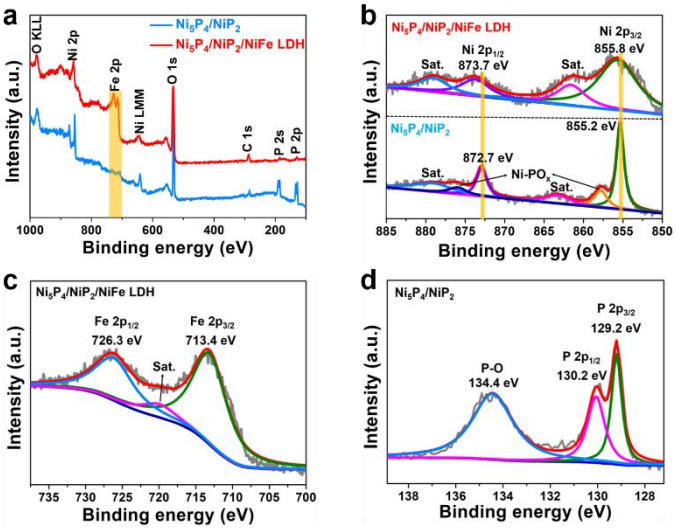

Fig. 2 (a) XPS spectra, and high-resolution XPS spectra of (b) Ni 2p for the Ni_5P_4/NiP_2 foam and $Ni_5P_4/NiP_2/NiFe$ LDH. High-resolution XPS spectra of (c) Fe 2p for the $Ni_5P_4/NiP_2/NiFe$ LDH, and (d) P 2p for the Ni_5P_4/NiP_2 foam.

intensity of P was quite weak for the $Ni_5P_4/NiP_2/NiFe$ LDH since XPS was only surface sensitive. The high-resolution Ni 2p spectrum of $Ni_5P_4/NiP_2/NiFe$ LDH (Fig. 2b) were fitted into two spin-orbit peaks at 873.7 and 855.8 eV accompanied by two broad satellite peaks (identified as "Sat."), corresponding to the Ni $2p_{1/2}$ and Ni $2p_{3/2}$, respectively. The high-resolution spectrum of Fe 2p in Fig. 2c showed a pair of peaks at 726.3 and 713.4 eV, which were assigned to the Fe $2p_{1/2}$ and Fe $2p_{3/2}$, respectively. All these features indicated the Ni^{2+} and Fe^{3+} oxidation states on the surface of the core-shell hybrids, confirming the formation of NiFe LDH.[29, 36, 37] For the Ni_5P_4/NiP_2 foam, the two spin-orbit peaks of Ni 2p were located at 872.7 and 855.2 eV (Fig. 2b), respectively, and the two small peaks at 857.6 and 875.5 eV were attributed to the Ni-PO_x due to the surface oxidation in air.[38] Fig. 2d shows the high-resolution spectrum of P 2p for the Ni_5P_4/NiP_2 foam, where the two peaks at 130.2 and 129.2 eV were assigned to the P $2p_{3/2}$ and P $2p_{1/2}$, respectively, and the peak at 134.4 eV was attributed to the oxidized P species.[16]

We then assessed the electrocatalytic OER activity of the $Ni_5P_4/NiP_2/NiFe$ LDH catalyst in 1 M KOH using a typical three-electrode system (see details in Supplementary Information). Fig. 3a displays the polarization curves of different electrodes, showing that our 3D core-shell electrode achieved current densities of 10, 100 and 300 mA cm^{-2} at extremely low overpotentials of 197, 243, and 283 mV, respectively, which were not only much better than that of Ni foam, Ni_5P_4/NiP_2 foam and pure NiFe LDH, but also outperformed the IrO_2 benchmark (225, 359, and 462 mV). Note that the anodic peak of Ni_5P_4/NiP_2 foam was attributed to the oxidation of Ni^{2+} to Ni^{3+}.[16, 39] Additionally, the OER activity of $Ni_5P_4/NiP_2/NiFe$ LDH with different electrodeposition time of NiFe LDH (Fig. S2 shows their SEM images) was also studied. As the polarization curves shown in Fig. S4, the one with electrodeposition time of 75 s possessed the highest OER activity. Fig. 3b shows the corresponding Tafel plots, from which

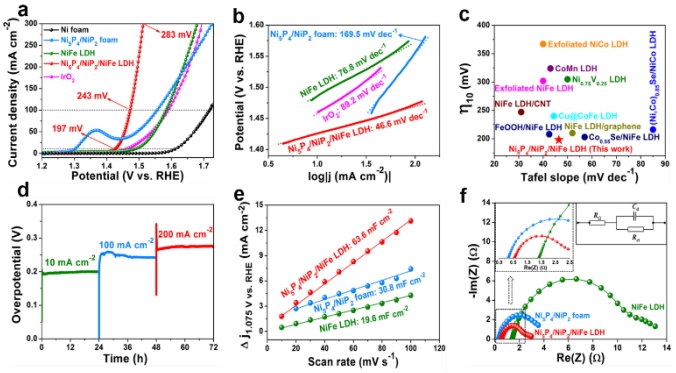

Fig. 3 OER performance conducted in 1 M KOH. (a) Polarization curves, and (b) corresponding Tafel plots of different electrodes. (c) Comparison of overpotential required at 10 mA cm^{-2} (η_{10}) and Tafel slope with other LDH-based OER electrocatalysts. (d) Chronopotentiometry curves of $Ni_5P_4/NiP_2/NiFe$ LDH at constant current densities of 10, 100, and 200 mA cm^{-2}. (e) Capacitive currents as a function of scan rate, and (f) Nyquist plots (overpotential = 250 mV) for the samples. The insets in (f) are the enlarged EIS curves of the squared parts and equivalent circuit for the EIS. References cited in panel (c): FeOOH/NiFe LDH,[40] $Co_{0.85}Se$/NiFe LDH,[41] $(Ni,Co)_{0.85}Se$/NiCo LDH,[42] NiFe LDH/CNT (carbon nanotube),[43] NiFe LDH/graphene,[44] Cu@CoFe LDH,[45] exfoliated NiFe LDH,[26] exfoliated NiCo LDH,[46] $Ni_{0.75}V_{0.25}$ LDH,[47] and CoMn LDH.[48]

we can see that the Tafel slope of the $Ni_5P_4/NiP_2/NiFe$ LDH hybrid was only 46.6 mV dec^{-1}, which was much smaller than that of Ni_5P_4/NiP_2 foam (169.5 mV dec^{-1}), pure NiFe LDH (76.8 mV dec^{-1}), and IrO_2 (89.2 mV dec^{-1}). These results establish our 3D core-shell electrode of $Ni_5P_4/NiP_2/NiFe$ LDH to be a low-cost and highly efficient OER catalyst that is superior to almost all LDH-based OER catalysts (Fig. 3c) as well as most reported high-performance electrocatalysts (see comparison details in Table S1). Impressively, as shown in Fig. 3d, the $Ni_5P_4/NiP_2/NiFe$ LDH catalyst also exhibited very good stability both under small (10 mA cm^{-2}) and large current densities (100 and 200 mA cm^{-2}). Moreover, as the SEM and TEM images shown in Fig. S5 and Fig. S6, respectively, the 3D hierarchical core-shell nanostructures for the $Ni_5P_4/NiP_2/NiFe$ LDH hybrid was perfectly preserved even after long-term stability tests, demonstrating the splendid mechanical and catalytic stability. Therefore, our 3D core-shell electrode is promising toward large-scale water electrolysis in view of the excellent performance and facile synthesis methods.

In order to figure out the mechanism of the enhanced OER activity for the $Ni_5P_4/NiP_2/NiFe$ LDH hybrid catalyst, electrochemically active surface area (ECSA) was estimated from the double-layer capacitance (C_{dl}) by carrying out cyclic voltammetry (CV) tests in the non-Faradaic region (Fig. S7). As shown in Fig. 3e, the 3D core-shell $Ni_5P_4/NiP_2/NiFe$ LDH electrode possessed the largest C_{dl} of 63.6 mF cm^{-2}, which was more than 2 times that of Ni_5P_4/NiP_2 foam (30.8 mF cm^{-2}) and 3.4 times that of pure NiFe LDH (19.6 mF cm^{-2}), manifesting the increased ECSA and more exposure of active sites contributed by the rational design of the 3D hierarchical core-shell nanoarchitectures. The large ECSA is favorable for water molecule adsorption and intimate contact with the electrolyte, along with abundant active sites for catalytic reactions, which definitely contribute to the enhanced activity.[29] Electrochemical impedance spectra (EIS) were also conducted to gain insights into the OER kinetics. Fig. 3f presents the Nyquist plots and corresponding equivalent circuit, which clearly revealed that the charge-transfer resistance (R_{ct}) of the $Ni_5P_4/NiP_2/NiFe$ LDH hybrid catalyst (1.2 Ω) was much smaller than that of Ni_5P_4/NiP_2 foam (3.9 Ω) and pure NiFe LDH (10.5 Ω), suggesting a faster electron transfer during the electrochemical reactions and thus a more efficient kinetics was favored by the smart core-shell electrode.[49] Meanwhile, the inset in Fig. 3f shows the enlarged Nyquist plots, which exhibited smaller series resistances (R_s) for the Ni_5P_4/NiP_2 foam and $Ni_5P_4/NiP_2/NiFe$ LDH hybrid compared with that of pure NiFe LDH/Ni foam, indicating high-quality electrical integration and robust contact of the catalysts with the subtrates.[29, 30] This was because the 3D conductive Ni_5P_4/NiP_2 foam was directly synthesized via thermal phosphorization of Ni foam, which retained the high integrity. And the NiFe LDH nanosheets intimately attached on the Ni_5P_4/NiP_2 microsheets, offering excellent electrical contacts and integrated 3D hierarchical nanostructures. Therefore, the outstanding OER performance of the 3D hierarchical core-shell electrode can be attributed to the following factors: (1) The robust contact of NiFe LDH shell with highly conductive Ni_5P_4/NiP_2 core enables excellent electrical connection and integrated 3D hierarchical nanostructures, providing an efficient pathway for electron transfer from the inner Ni_5P_4/NiP_2 microsheets to the outer NiFe LDH nanosheets. (2) The 2D NiFe LDH nanosheets vertically grow on the rough surface of 3D

Ni_5P_4/NiP_2 foam, leaving numerous exposed edges, which offers more active edge sites for catalytic reactions. (3) The smart 3D hierarchical core-shell nanostructures provide a large surface area with high porosity, which greatly facilitate water molecule adsorption, electrolyte diffusion, and gaseous products releasing. (4) It has been demonstrated that amorphous materials generally exhibit higher OER activity than that of crystalline ones due to a larger amount of randomly oriented bonds and a greater density of surface unsaturated sites, which enhance the adsorption of reactants.[20]

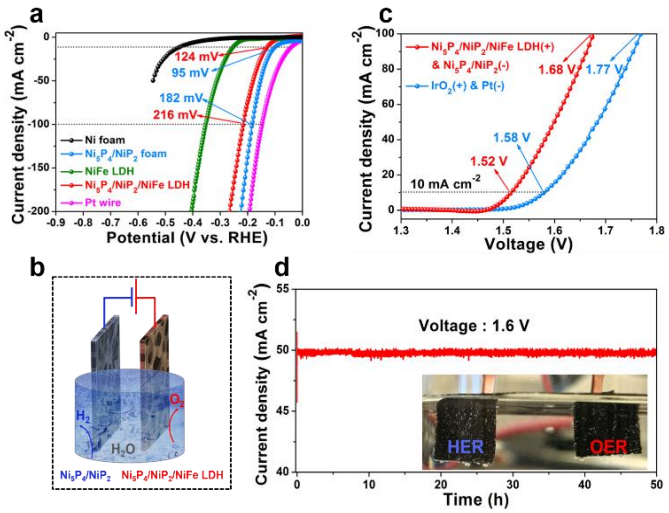

Fig. 4 HER and overall water splitting performance in 1 M KOH. (a) HER polarization curves of different electrodes. (b) Schematic illustration of the electrolyzer using Ni_5P_4/NiP_2 foam and Ni_5P_4/NiP_2/NiFe LDH as cathode and anode, respectively. (c) Polarization curves of overall water splitting at room temperature. (d) Long-term stability test conducted at constant voltage of 1.6 V. (The inset is the optical photograph showing the generation of H_2 and O_2 bubbles on the electrodes.)

Since NiFe LDH catalysts are also reported to be active for hydrogen evolution reaction (HER) in the alkaline electrolytes,[24, 29, 44] we further evaluated the HER performance for the as-prepared electrodes, which was also conducted in 1 M KOH via a three-electrode cell comprising a graphite foil as the counter electrode. As shown in Fig. 4a, the Ni_5P_4/NiP_2/NiFe LDH hybrid electrode delivered current densities of 10 and 100 mA cm^{-2} at overpotentials of 124 and 216 mV, respectively, showing much higher HER activity than that of pure NiFe LDH due to more active edge sites and efficient electron transfer. However, this performance was worse than that of Ni_5P_4/NiP_2 foam, which has been demonstrated to be an efficient HER catalysts both in acidic and alkaline media.[38, 50, 51] It yielded current densities of 10 and 100 mA cm^{-2} at overpotentials of 95 and 182 mV, respectively, which was very close to the HER benchmark of Pt wire. Hence, as illustrated in Fig. 4b, we further combined our 3D core-shell Ni_5P_4/NiP_2/NiFe LDH catalyst (anode) with Ni_5P_4/NiP_2 foam (cathode) to fabricate a two-electrode cell for overall water splitting in 1 M KOH. Attractively, the powerful combination delivered current densities of 10 and 100 mA cm^{-2} at small voltages of 1.52 and 1.68 V at room temperature (Fig. 4c), which was much better than the benchmark of IrO_2/Pt (1.58 and 1.77 V). Furthermore, the two catalysts were very stable during overall water splitting. As shown in Fig. 4d, the current density totally showed no decay under a constant voltage of 1.6 V during 50 h electrolysis, exhibiting great potentials for large-scale applications.

Conclusions

In summary, we have designed a 3D hierarchical core-shell nanostructured electrocatalyst by growing NiFe LDH nanosheets on highly conductive Ni_5P_4/NiP_2 nanoarrays via a facile and scalable methods. Benefited from the unique 3D hierarchical core-shell nanostructure and good electrical conductivity rendered by the inner Ni_5P_4/NiP_2 foam, the novel hybrid catalyst showed a large surface area with abundant active edge sites, efficient electron transfer, and robust integrated structure, all of which led to the final outstanding OER performance. Our work not only opens up the possibility to engineer 2D layered materials into efficient electrocatalysts but also presents a new and affordable approach to design 3D hierarchical hybrid electrodes for energy storage and conversion.

Acknowledgements

The work performed at the University of Houston is funded by the US Department of Energy under Award Number DE-SC0010831, and that in China is supported by the China Scholarship Council, the National Natural Science Foundation of China (No. 21377044 and 21573085), and the excellent doctorial dissertation cultivation grant (No. 2017YBZZ075) from Central China Normal University.

References

1 L. Yu, Y. Xie, J. Zhou, Y. Li, Y. Yu and Z. Ren, *J. Mater. Chem. A*, 2018, **6**, 4706-4713.
2 Z. W. Seh, J. Kibsgaard, C. F. Dickens, I. Chorkendorff, J. K. Nørskov and T. F. Jaramillo, *Science*, 2017, **355**, 4998-5009.
3 L. Yu, G. Li, X. Zhang, X. Ba, G. Shi, Y. Li, P. K. Wong, J. C. Yu and Y. Yu, *ACS Catal.*, 2016, **6**, 6444-6454.
4 M. W. Kanan and D. G. Nocera, *Science*, 2008, **321**, 1072-1075.
5 F. Yu, H. Zhou, Z. Zhu, J. Sun, R. He, J. Bao, S. Chen and Z. Ren, *ACS Catal.*, 2017, **7**, 2052-2057.
6 W. Chen, Y. Liu, Y. Li, J. Sun, Y. Qiu, C. Liu, G. Zhou and Y. Cui, *Nano Lett.*, 2016, **16**, 7588-7596.
7 S. H. Ye, Z. X. Shi, J. X. Feng, Y. X. Tong and G. R. Li, *Angew. Chem. Int. Ed.*, 2018, **57**, 1-6.
8 J. Jiang, Q. Liu, C. Zeng and L. Ai, *J. Mater. Chem. A*, 2017, **5**, 16929-16935.
9 H. Liang, A. N. Gandi, D. H. Anjum, X. Wang, U. Schwingenschlögl and H. N. Alshareef, *Nano Lett.*, 2016, **16**, 7718-7725.
10 X. Long, H. Lin, D. Zhou, Y. An and S. Yang, *ACS Energy Lett.*, 2018, **3**, 290-296.
11 T. Tang, W. J. Jiang, S. Niu, N. Liu, H. Luo, Y. Y. Chen, S. F. Jin, F. Gao, L. J. Wan and J. S. Hu, *J. Am. Chem. Soc.*, 2017, **139**, 8320-8328.
12 X. Li, Z. Niu, J. Jiang and L. Ai, *J. Mater. Chem. A*, 2016, **4**, 3204-3209.
13 Y. Li, F. M. Li, X. Y. Meng, S. N. Li, J. H. Zeng and Y. Chen, *ACS Catal.*, 2018, **8**, 1913-1920.
14 J. Yin, Y. Li, F. Lv, M. Lu, K. Sun, W. Wang, L. Wang, F. Cheng, Y. Li and P. Xi, *Adv. Mater.*, 2017, **29**, 1704681.

15 S. H. Yu, C. Gu, S. Hu, X. Zheng, M. R. Gao, Y. R. Zheng, L. Shi, Q. Gao, X. Zheng and W. Chu, *Angew.Chem.*, 2018, **130**, 4084-4088.
16 M. Wang, M. Lin, J. Li, L. Huang, Z. Zhuang, C. Lin, L. Zhou and L. Mai, *Chem. Commun.*, 2017, **53**, 8372-8375.
17 X. Liu, J. Jiang and L. Ai, *J. Mater. Chem. A*, 2015, **3**, 9707-9713.
18 Y. Jin, S. Huang, X. Yue, H. Du and P. K. Shen, *ACS Catal.*, 2018, **8**, 2359-2363.
19 Z. Fang, L. Peng, H. Lv, Y. Zhu, C. Yan, S. Wang, P. Kalyani, X. Wu and G. Yu, *ACS Nano*, 2017, **11**, 9550-9557.
20 H. Liang, A. N. Gandi, C. Xia, M. N. Hedhili, D. H. Anjum, U. Schwingenschlögl and H. N. Alshareef, *ACS Energy Lett.*, 2017, **2**, 1035-1042.
21 Y. Zhao, X. Jia, G. I. Waterhouse, L. Z. Wu, C. H. Tung, D. O'Hare and T. Zhang, *Adv. Energy Mater.*, 2016, **6**, 1502585.
22 Y. Zhao, Y. Zhao, G. I. Waterhouse, L. Zheng, X. Cao, F. Teng, L. Z. Wu, C. H. Tung, D. O'Hare and T. Zhang, *Adv. Mater.*, 2017, **29**, 1703828.
23 Y. Yang, L. Dang, M. J. Shearer, H. Sheng, W. Li, J. Chen, P. Xiao, Y. Zhang, R. J. Hamers and S. Jin, *Adv. Energy Mater.*, 2018, DOI: 10.1002/aenm.201703189.
24 J. Luo, J. H. Im, M. T. Mayer, M. Schreier, M. K. Nazeeruddin, N. G. Park, S. D. Tilley, H. J. Fan and M. Grätzel, *Science*, 2014, **345**, 1593-1596.
25 Y. Wang, Y. Zhang, Z. Liu, C. Xie, S. Feng, D. Liu, M. Shao and S. Wang, *Angew. Chem. Int. Ed.*, 2017, **56**, 5867-5871.
26 F. Song and X. Hu, *Nat. Commun.*, 2014, **5**, 4477.
27 Y. Wang, C. Xie, Z. Zhang, D. Liu, R. Chen and S. Wang, *Adv. Funct. Mater.*, 2018, **28**, 1703363.
28 C. Qiu, L. Ai and J. Jiang, *ACS Sustainable Chem. Eng.*, 2018, **6**, 4492-4498.
29 L. Yu, H. Zhou, J. Sun, F. Qin, F. Yu, J. Bao, Y. Yu, S. Chen and Z. Ren, *Energy Environ. Sci.*, 2017, **10**, 1820-1827.
30 H. Zhou, F. Yu, J. Sun, H. Zhu, I. K. Mishra, S. Chen and Z. Ren, *Nano Lett.*, 2016, **16**, 7604-7609.
31 M. S. Faber and S. Jin, *Energy Environ. Sci.*, 2014, **7**, 3519-3542.
32 H. Wang, D. Kong, P. Johanes, J. J. Cha, G. Zheng, K. Yan, N. Liu and Y. Cui, *Nano Lett.*, 2013, **13**, 3426-3433.
33 M. Cabán-Acevedo, M. L. Stone, J. Schmidt, J. G. Thomas, Q. Ding, H. C. Chang, M. L. Tsai, J. H. He and S. Jin, *Nat. Mater.*, 2015, **14**, 1245.
34 H. Liang, L. Li, F. Meng, L. Dang, J. Zhuo, A. Forticaux, Z. Wang and S. Jin, *Chem. Mater.*, 2015, **27**, 5702-5711.
35 H. Zhou, F. Yu, J. Sun, R. He, S. Chen, C.-W. Chu and Z. Ren, *Proc. Natl. Acad. Sci. U. S. A.*, 2017, **114**, 5607-5611.
36 Y. Y. Chen, Y. Zhang, X. Zhang, T. Tang, H. Luo, S. Niu, Z. H. Dai, L. J. Wan and J. S. Hu, *Adv. Mater.*, 2017, **29**, 1703311.
37 X. Han, C. Yu, J. Yang, C. Zhao, H. Huang, Z. Liu, P. M. Ajayan and J. Qiu, *Adv. Mater. Interfaces*, 2016, **3**, 1500782.
38 I. K. Mishra, H. Zhou, J. Sun, K. Dahal, Z. Ren, R. He, S. Chen and Z. Ren, *Mater. Today Phys.*, 2018, **4**, 1-6.
39 G. F. Chen, T. Y. Ma, Z. Q. Liu, N. Li, Y. Z. Su, K. Davey and S. Z. Qiao, *Adv. Funct. Mater.*, 2016, **26**, 3314-3323.
40 J. Chi, H. Yu, B. Qin, L. Fu, J. Jia, B. Yi and Z. Shao, *ACS Appl. Mater. Interfaces*, 2016, **9**, 464-471.
41 Y. Hou, M. R. Lohe, J. Zhang, S. Liu, X. Zhuang and X. Feng, *Energy Environ. Sci.*, 2016, **9**, 478-483.
42 C. Xia, Q. Jiang, C. Zhao, M. N. Hedhili and H. N. Alshareef, *Adv. Mater.*, 2016, **28**, 77-85.
43 M. Gong, Y. Li, H. Wang, Y. Liang, J. Z. Wu, J. Zhou, J. Wang, T. Regier, F. Wei and H. Dai, *J. Am. Chem. Soc.*, 2013, **135**, 8452-8455.
44 Y. Jia, L. Zhang, G. Gao, H. Chen, B. Wang, J. Zhou, M. T. Soo, M. Hong, X. Yan and G. Qian, *Adv. Mater.*, 2017, **29**, 1700017.
45 L. Yu, H. Zhou, J. Sun, F. Qin, D. Luo, L. Xie, F. Yu, J. Bao, Y. Li and Y. Yu, *Nano Energy*, 2017, **41**, 327-336.
46 H. Liang, F. Meng, M. Cabán-Acevedo, L. Li, A. Forticaux, L. Xiu, Z. Wang and S. Jin, *Nano Lett.*, 2015, **15**, 1421-1427.
47 K. Fan, H. Chen, Y. Ji, H. Huang, P. M. Claesson, Q. Daniel, B. Philippe, H. Rensmo, F. Li and Y. Luo, *Nat. Commun.*, 2016, **7**, 11981.
48 F. Song and X. Hu, *J. Am. Chem. Soc.*, 2014, **136**, 16481-16484.
49 X. Li, W. Liu, M. Zhang, Y. Zhong, Z. Weng, Y. Mi, Y. Zhou, M. Li, J. J. Cha and Z. Tang, *Nano Lett.*, 2017, **17**, 2057-2063.
50 X. Wang, Y. V. Kolen'ko, X. Q. Bao, K. Kovnir and L. Liu, *Angew. Chem. Int. Ed.*, 2015, **54**, 8188-8192.
51 X. Wang, W. Li, D. Xiong, D. Y. Petrovykh and L. Liu, *Adv. Funct. Mater.*, 2016, **26**, 4067-4077.

Journal Name

ARTICLE

The table of contents entry

Amorphous NiFe LDH nanosheets were decorated on nickel phosphide nanoarrays to form a 3D core-shell electrocatalyst for efficient water oxidation.

TOC Figure